Rheol Acta (2011) 50:317–326
DOI 10.1007/s00397-010-0519-9

ORIGINAL CONTRIBUTION

Mircorheology and jamming in a yield-stress fluid

F. K. Oppong · J. R. de Bruyn

Received: 29 April 2010 / Revised: 18 November 2010 / Accepted: 22 December 2010 / Published online: 18 March 2011
© Springer-Verlag 2011

Abstract We study the onset of a yield stress in a polymer microgel dispersion using a combination of particle-tracking microrheology and shear rheometry. On the bulk scale, the dispersion changes from a predominantly viscous fluid to a stiff elastic gel as the concentration of the microgel particles increases. On the microscopic scale, the tracer particles see two distinct microrheological environments over a range of concentrations—one being primarily viscous, the other primarily elastic. The fraction of the material that is elastic on the microscale increases from zero to one as the concentration increases. Our results indicate that the yield stress appears as the result of jamming of the microgel particles, and we infer a model for the small-scale structure and interactions within the dispersion and their relationship to the bulk viscoelastic properties.

This paper was presented at Viscoplastic Fluids: From Theory to Application, November 1–5, 2009, Limassol, Cyprus.

F. K. Oppong · J. R. de Bruyn (✉)
Department of Physics and Astronomy,
University of Western Ontario, London,
ON, Canada N6A 3K7
e-mail: debruyn@uwo.ca

F. K. Oppong
Unilever Research and Development,
Colworth Science Park Sharnbrook,
Bedfordshire, MK44 1LQ, UK

Keywords Yield stress · Structure · Microgel · Jamming

Introduction

The bulk mechanical properties of any complex fluid derive from its small-scale structure, but it is often difficult to make clear connections between the microstructure and the bulk behaviour. Particle-tracking microrheology (Mason and Weitz 1995; Mason 2000; Valentine et al. 2001; Wong et al. 2004; Waigh 2005; Gardel et al. 2005; Oppong et al. 2006; Oppong and de Bruyn 2007; de Bruyn and Oppong 2010) is a recently-developed technique which allows determination of the micron-scale linear viscoelastic properties of a complex fluid from analysis of the thermally driven diffusive motion of suspended tracer particles. When the tracer particles are much larger than the characteristic structural length scale of the fluid, microrheology will simply measure the bulk rheological behaviour, but if the particles are small compared to any structure, microrheological measurements probe the local environment in which the particles move. Particle-tracking microrheology has been used to study several different kinds of complex fluids, including a variety of gels (Oppong et al. 2006, 2008; Oppong and de Bruyn 2007; Gao and Kilfoil 2007; Caggioni et al. 2007; Houghton et al. 2008).

In this paper, we use particle-tracking microrheology and shear rheometry to study the viscoelastic properties of aqueous dispersions of Carbopol (Noveon 2002), an important commercial product that is used extensively as a rheology modifier. Carbopol is a polymer microgel which forms a transparent yield-stress gel at very low concentrations (Piau 2007). Microgel dispersions

consist of small particles of cross-linked polymer molecules suspended in a solvent. Individual microgel particles are porous and deformable, with a size which can depend dramatically on their physical or chemical environment. For example, the size of a microgel particle can be tuned by changing the polymer–polymer and polymer–solvent interactions, the pH, or the temperature (Saunders and Vincent 1999; Pelton 2000; Lyon et al. 2004; Das et al. 2006). The interesting structure and thermodynamic properties of well-characterized microgel materials such as poly-*N*-isopropylacrylamide (poly-NIPAM) have been extensively studied (Senff and Richtering 1999a, b; Levin et al. 2002; Denton 2003; Wu et al. 2003; Gottwald et al. 2004; Gottwald et al. 2005; Crassous et al. 2006). Dilute suspensions of microgel particles display rheological behaviour similar to that of dilute hard-sphere colloidal suspensions (Borrega et al. 1999; Cloitre et al. 2003a, b), but at higher concentrations they are viscoplastic with a concentration-dependent yield stress (Piau 2007). Industrial microgels such as Carbopol are less well characterized than model materials such as poly-NIPAM, but it is nonetheless important to understand their microstructure and properties.

The combination of bulk and microrheological measurements used in the work reported here allows us to compare and study correlations between bulk and microscopic material properties. In previous microrheological studies on Carbopol (Oppong et al. 2006; Oppong and de Bruyn 2007), we showed that the dispersions were inhomogeneous on the microscopic scale, and that the suspended tracer particles could be separated into populations which experienced different rheological microenvironments. We also speculated on the connection between the microscopic material properties and the bulk yield stress (Oppong and de Bruyn 2007). In the present paper, we extend our previous work to study the microrheology of Carbopol as a function of concentration, ranging from extremely low concentrations at which the dispersions are viscous, to higher concentrations at which they are stiff gels. We link Carbopol's microscopic behaviour, as probed by our microrheological measurements, with the bulk behaviour probed by shear rheometry. The combination of the two techniques allows us to develop a physical picture for the microstructure of this material. We show that the onset of yield-stress behaviour results from jamming of the swollen microgel particles (Lally et al. 2007; Prasad et al. 2003), and we are able to follow the progress of the jamming transition on both bulk and microscopic length scales.

Experiment

We study aqueous dispersions of Carbopol ETD 2050 (Noveon 2002) for concentrations c in the range 0.01 wt.% $\leq c \leq$ 1.0 wt.%. This form of Carbopol was chosen because it produces gels which are particularly clear. Our samples were prepared by adding Carbopol powder to continuously stirred deionized water containing 5×10^{-5} by volume fluorescent latex microspheres with a diameter $2a = 1.0$ μm. The dispersion initially had a pH around 3. NaOH was added to raise the pH to 6, at which value the bulk rheological properties of Carbopol do not depend strongly on pH. The dispersions were mixed with a propeller-blade mixer for up to 8 h to ensure homogeneity (Tabuteau et al. 2007) and uniform distribution of the tracer microspheres. We verified that the presence of the microspheres did not affect the bulk rheology of the material.

Carbopol consists of particles of cross-linked poly(acrylic acid). Observations with an optical microscope indicated that the particles are roughly 1 μm in diameter when dry and on average about 2 μm in diameter, and significantly polydisperse, when initially dispersed in water. When the pH is neutralized the molecules become charged, and the osmotic pressure of the counter-ions causes the particles to swell substantially (Cloitre et al. 2003a, b). They also become invisible under the microscope.

The thermally driven motion of the fluorescent tracer particles in the Carbopol was tracked using a CCD camera on an inverted fluorescence microscope with a × 40 objective. Images with a spatial resolution of 0.33 μm/pixel were recorded at a rate of ten frames per second for about 10 s, the length of the recording being limited by the memory of the computer system used. Each image included roughly 50 tracer particles. The particle trajectories were determined using the image analysis software described in (Crocker and Grier 1996; Crocker and Weeks 2008). This software locates particles in each image and tracks their motion from one image to the next. The microscopic viscous and elastic moduli of the material were calculated as a function of frequency ω from the mean squared displacement $\langle r^2(1/\omega)\rangle$ of the tracers using the fluctuation–dissipation theorem and a generalized Stokes–Einstein relation, as described in detail in (Mason and Weitz 1995; Mason 2000; Valentine et al. 2001; Gardel et al. 2005). If the tracer particles were moving purely diffusively, $\langle r^2(1/\omega)\rangle$ would increase linearly with time. In contrast, if the particles were confined in a purely

elastic medium, $\langle r^2(1/\omega)\rangle$ would be constant for low enough frequencies (long enough lag times). Particles in a viscoelastic medium would display intermediate behaviour. Briefly, we define $\alpha(\omega)$ to be the local logarithmic slope of the mean squared displacement as a function of lag time τ,

$$\alpha(\omega) = \left.\frac{d\ \ln\langle r^2(\tau)\rangle}{d\ \ln\tau}\right|_{\tau=1/\omega}. \tag{1}$$

The magnitude of the mechanical modulus is then calculated as (Mason 2000)

$$|G(\omega)| = \frac{k_B T}{\pi a \langle r^2(1/\omega)\rangle \Gamma\,(1+\alpha(\omega))}, \tag{2}$$

where k_B is the Boltzmann constant, T the temperature, a the radius of the tracer particle, and Γ the Gamma function. The viscous modulus G'' is then given by

$$G''(\omega) = |G(\omega)| \sin\left(\frac{\pi\alpha(\omega)}{2}\right) \tag{3}$$

and the elastic modulus G' by

$$G'(\omega) = |G(\omega)| \cos\left(\frac{\pi\alpha(\omega)}{2}\right). \tag{4}$$

Bulk rheological measurements were made using an Ares RHS strain-controlled rheometer with a 50-mm diameter cone-and-plate measuring geometry. Fine emery paper was glued to the tools to prevent wall slip. The bulk viscous and elastic moduli were determined by applying a small-amplitude oscillatory shear to the material and measuring the response. Yield stress was determined from steady shear experiments, in which the steady state stress is measured as a function of strain rate. All measurements were performed at 25°C.

Results

From the trajectories of the tracer particles determined by the image processing software, we calculate the one-dimensional mean squared displacement of the tracer particles, averaged over all particles and all independent starting times t, given by $\langle x^2(\tau)\rangle_e = \langle |x(t+\tau) - x(t)|^2\rangle$ where τ is the lag time. This quantity is plotted in Fig. 1 for Carbopol concentrations ranging from 0.01 to 1.0 wt.%. $\langle x^2(\tau)\rangle_e$ is approximately described by a power-law dependence on τ over the range of lag times covered in our experiments, i.e. $\langle x^2(\tau)\rangle_e \sim \tau^\alpha$ for a given c. Careful examination of Fig. 1 shows

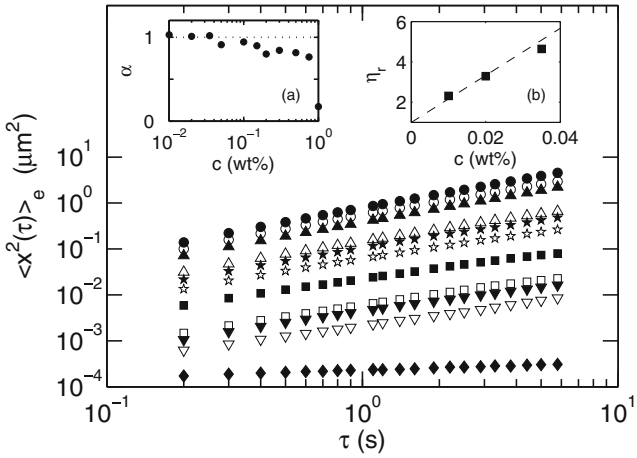

Fig. 1 The one-dimensional ensemble-averaged mean squared displacement $\langle x^2(\tau)\rangle_e$ of the tracer particles for several different values of the concentration c. From *top* to *bottom*, $c = 0.01$, 0.02, 0.035, 0.05, 0.075, 0.10, 0.15, 0.2, 0.3, 0.5, and 1.0 wt.%. *Inset a* shows the power-law exponent α as a function of c. The *dotted line* is $\alpha = 1$. *Inset b* shows the viscosity relative to that of water for the lowest concentrations. The *line* is a fit to Einstein's equation for the viscosity of a suspension of hard spheres

that the data have a slight curvature, i.e. the power-law exponent α varies slightly over the experimental range of τ. At a fixed value of τ, $\langle x^2(\tau)\rangle_e$ decreases with increasing concentration. Inset (a) of Fig. 1 shows the mean power-law exponent α as a function of c, determined by averaging the τ-dependent exponents obtained from fitting to consecutive triplets of data points in the range $0.2 < \tau < 5$ s. The standard deviation in these exponent values is typically less than ± 0.05. For $c \lesssim 0.035$ wt.%, we find that $\alpha = 1$ within experimental uncertainties, indicating that at these low concentrations, the tracers diffuse in an environment that is purely viscous within the precision of our measurements. At higher concentrations, however, α decreases as the material becomes viscoelastic. At $c = 1.0$ wt.%, α drops sharply and $\langle x^2(\tau)\rangle_e$ becomes almost independent of τ, indicating that at this concentration the tracer particles are strongly confined in a predominantly elastic environment.

At concentrations low enough that the Carbopol dispersion behaves as a dilute suspension of hard spheres (Cloitre et al. 2003a, b) and the microgel particles move diffusively, we can use the Stokes–Einstein relation to determine the viscosity from $\langle x^2(\tau)\rangle_e$. The results are plotted in inset (b) of Fig. 1. The viscosity η_r of a suspension of colloidal particles relative to that of the background fluid (here water) is in turn given by Einstein's equation, $\eta_r = 1 + 2.5\phi$ (Einstein

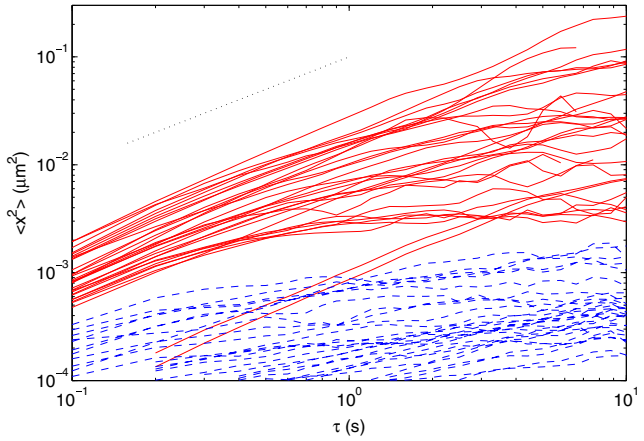

Fig. 2 The mean squared displacements of the individual particles tracked at $c = 0.3$ wt.%. The particles are labelled as fast or slow on the basis of their value of $\alpha = d\ln\langle x^2(\tau)\rangle / d\ln\tau$, evaluated for $0.3 \le \tau \le 0.5$ s. *Solid lines* indicate particles in the fast population, and *dashed lines*, those in the slow population. The *straight dotted line* has a logarithmic slope of 1

1906), where ϕ is the volume fraction of the particles. Fitting this to the viscosity data plotted in Fig. 1b, we can extract a relationship, valid at low concentrations, between c and ϕ for our Carbopol dispersion. We find $\phi = (4,300 \pm 500)c$. Using this result and taking the density of the dry Carbopol particles to be 1.47 g/cm^3 (Piau 2007), we calculate that they swell by a factor of 18 in diameter in the neutralized dispersion relative to their size when dry, or by a factor of nine in diameter (a factor of 790 in volume) relative to their size at a pH of 3. This is likely an overestimate because the Carbopol particles are porous rather than being hard spheres (Yu and Kaloni 1988), but nonetheless this simple result suggests that when neutralized, the Carbopol particles expand greatly, and so must consist of a very extended, tenuous network of polymer chains with a diameter of roughly 20 μm.

We have also performed small-angle light scattering experiments on pH-neutralized Carbopol (Lee et al. 2011). Although the details of this work will be reported elsewhere, the results of these experiments indicate the presence of objects with a length scale of approximately 0.5 μm, independent of pH, and also a much larger length scale on the order of 20 μm (Lee et al. 2011). This larger length scale is consistent with the size of the microgel particles inferred from the viscosity data discussed above.

The data plotted in Fig. 1 were obtained by averaging over all recorded tracer particles. Carbopol gels are known to be heterogeneous on the micron length scale, however (Oppong et al. 2006; Oppong and de Bruyn 2007), in which case different tracer particles will see different material properties. To get information on the small-scale rheological environments probed by the individual tracer particles (Valentine et al. 2001; Liu et al. 2006; Oppong and de Bruyn 2007), we examine their individual mean squared displacements (which in this case are averaged over all starting times for a single particle). The results obtained at a concentration of 0.3 wt.% are shown in Fig. 2. The mean squared displacements appear to the eye to separate naturally into two distinct populations, plotted as solid and dashed lines in Fig. 2. The group of particles represented by the dashed lines exhibits a relatively slow increase in $\langle x^2(\tau)\rangle$, with a logarithmic slope significantly less than 1, over most of the range of τ. We refer to this group as the slow population of particles. In contrast, the mean squared displacements of the particles shown by the solid lines are significantly larger and show a near-linear increase with τ up to $\tau \approx 0.5$ s. We refer to this as the fast population. At higher τ the behaviour of $\langle x^2(\tau)\rangle$ for the fast particles becomes significantly sublinear as the motion of the tracer particles becomes restricted by the microstructure of the material, as discussed in detail in (Oppong et al. 2006; Oppong and de Bruyn 2007). To analyse these data, we determine the logarithmic slope of $\langle x^2(\tau)\rangle_e$ over a limited range of τ from 0.3 to 0.5 s. In this range, the fast particles in Fig. 2 move essentially diffusively, while the slow particles are strongly subdiffusive.

Figure 3 shows the distributions $N(\alpha)$ of the power-law exponents obtained from similar data for several concentrations. We find that for low c, $N(\alpha)$ shows a single peak close to $\alpha = 1$, indicating that all particles see a viscous and essentially homogeneous environment over the range of τ being considered. At $c =$

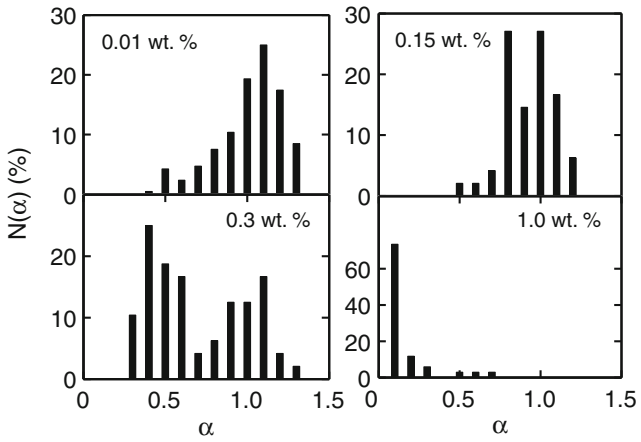

Fig. 3 The distribution $N(\alpha)$ derived from the squared displacements of the individual tracer particles for $c = 0.01$, 0.15, 0.30, and 1.0 wt.%

0.15, a second peak at $\alpha < 1$ appears. As c is increased further, the histograms show two peaks—the peak near $\alpha = 1$ remains, while the second peak moves to smaller values of α as c increases. The presence of two peaks in the distribution indicates the presence of two distinct microscopic environments within the dispersion: the tracers for which $\alpha \sim 1$ are moving in a viscous fluid over the relevant time scale, while the others see an increasingly viscoelastic environment. Finally, at $c =$ 1.0 wt.% the peak at $\alpha = 1$ disappears and the distribution has a single peak at a very low value of α, indicating a homogeneous, strongly elastic environment.

Based on these results, we label the tracer particles having α in the peak near $\alpha = 1$ as fast, while all others are slow. Figure 4 shows the mean values of the diffusive exponents for these two populations as a function of concentration: $\langle \alpha_f \rangle$ for the fast particles and $\langle \alpha_s \rangle$ for the slow. We find that $\langle \alpha_f \rangle = 1.0$ within uncertainties, independent of c. The peak due to the slow population first becomes distinguishable at $c =$ 0.15 wt.%, and $\langle \alpha_s \rangle$ decreases from 0.6 to almost zero as c increases. Concurrently, the fraction of the particles in the slow population, shown in the inset to Fig. 4, increases from zero to almost 100% at $c = 1.0$ wt.%.

Figure 5 shows the mean squared displacements $\langle x^2(\tau) \rangle_f$ and $\langle x^2(\tau) \rangle_s$ calculated for the fast and slow populations, respectively, for $0.2 \le c \le 1.0$ wt.%. The inset shows the dependence of these quantities on concentration at a particular value of the lag time, $\tau = 1$ s. For concentrations below 0.15 wt.%, only the fast population is observable. In this range of c, $\langle x^2(\tau) \rangle_f$ decreases steadily as c increases. At $c = 0.15$ wt.%

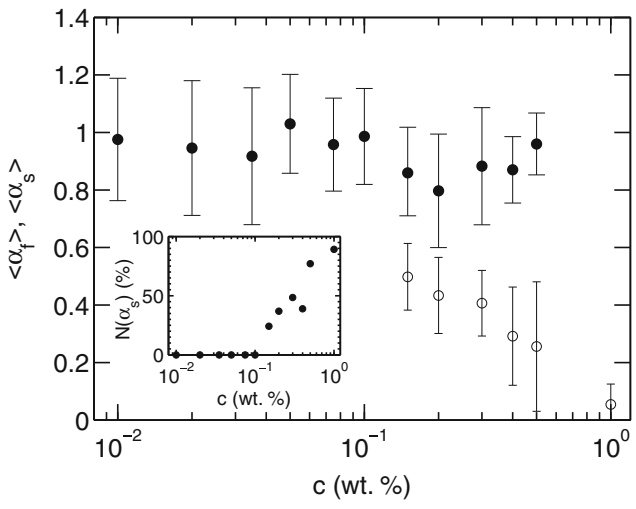

Fig. 4 The average diffusive exponent for the fast (α_f, *filled circles*) and slow (α_s, *empty circles*) populations. The *error bars* are standard deviations. The *inset* shows the fraction of particles in the slow population as a function of concentration

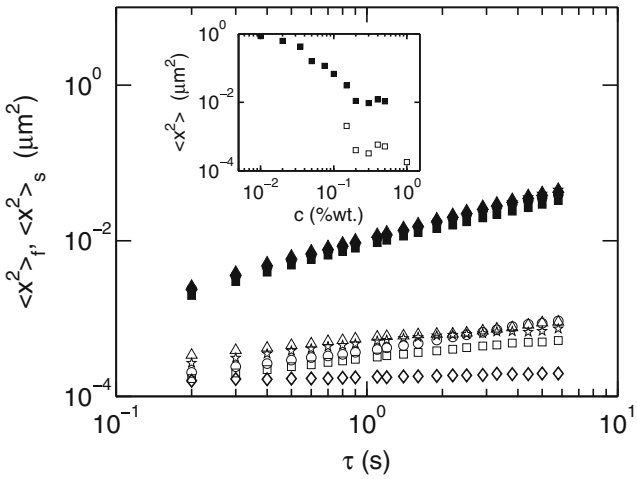

Fig. 5 The population-averaged mean squared displacement for the fast (*filled symbols*) and slow (*empty symbols*) particles for several concentrations. The *circles*, *squares*, *triangles*, *stars*, and *diamonds* represent $c =$ 0.2, 0.3, 0.4, 0.5, and 1.0 wt.%, respectively. The *inset* shows the variation with c of $\langle x^2(\tau) \rangle_f$ (*filled squares*) and $\langle x^2(\tau) \rangle_s$ (*empty squares*) at $\tau = 1$ s

the slow population becomes evident. For $0.2 \le c \le$ 0.5 wt.%, when the two populations are present, both $\langle x^2(\tau) \rangle_f$ and $\langle x^2(\tau) \rangle_s$ are independent of c within the experimental scatter. At $c = 1.0$ wt.% only the slow population remains.

Even the fast particles move at most 1 μm over the time we track them, so the motion of each particle is determined by the viscoelastic properties of the material in a small region that extends a distance of order a from the particle. We calculate the micron-scale viscous and elastic moduli $G''_m(\omega)$ and $G'_m(\omega)$ of the fast and slow environments from the population-averaged mean squared displacements $\langle x^2(\tau) \rangle_f$ and $\langle x^2(\tau) \rangle_s$ using Eqs. 3 and 4, as described in (Mason 2000). In these calculations, α is calculated numerically from the data as a function of τ. The results for three representative Carbopol concentrations are plotted as a function of frequency ω in Fig. 6. For $c < 0.05$ wt.%, the viscous modulus G''_m dominates and the elastic modulus is unmeasurable. This is illustrated by data for $c = 0.01$ wt.%, which are shown as circles in Fig. 6. At higher concentrations some elasticity is observed, as shown by the squares in Fig. 6 for $c = 0.1$ wt.%. For $0.15 \le c \le 0.5$ wt.%, the fast population (triangles in Fig. 6, measured at $c = 0.3$ wt.%) probes an environment that is predominantly viscous, and $G''_m > G'_m$ over the accessible frequency range. In contrast, at the same concentration the slow environment has $G'_m > G''_m$ over most of the frequency range (diamonds in Fig. 6), indicating that the slow population of particles sees a solid-like environment in which elastic effects dominate. In

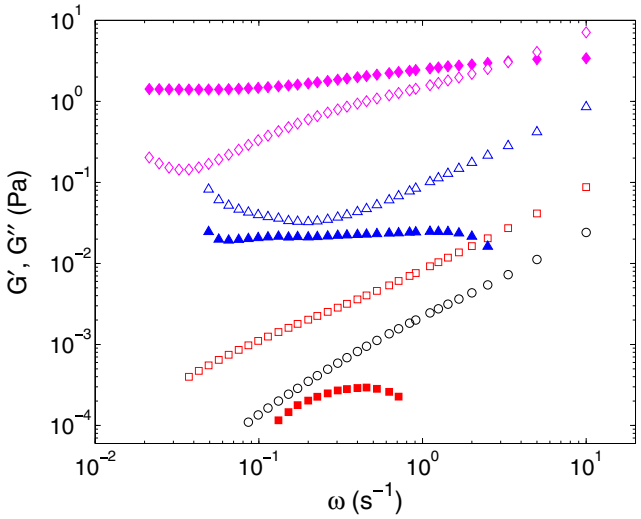

Fig. 6 The microscopic viscous and elastic moduli for Carbopol concentrations of $c = 0.01$ wt.% (*circles*), 0.1 wt.% (*squares*), and the fast and slow populations at 0.3 wt.% (*triangles* and *diamonds*, respectively). The *empty and filled symbols* are G'' and G', respectively. For the 0.01 wt.% dispersion, G' is too small to be measurable and only G'' is plotted

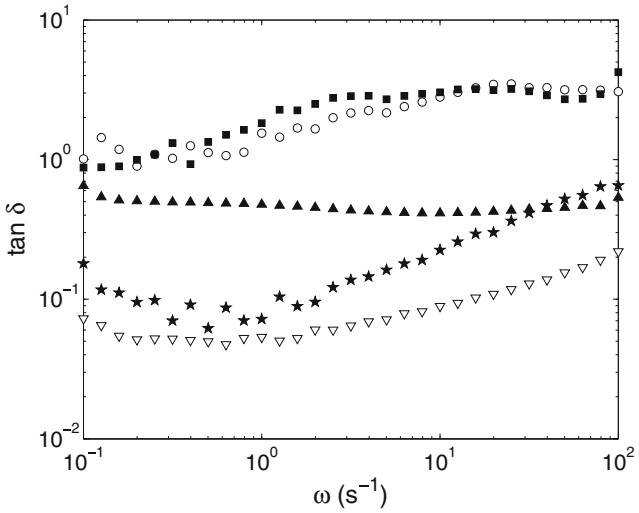

Fig. 7 $\tan\delta$, the ratio of the bulk viscous modulus to the elastic modulus, plotted as a function of angular frequency. *Circles*, $c = 0.04$ wt.%; *squares*, 0.05 wt.%; *upward-pointing triangles*, 0.08 wt.%; *stars*, 0.1 wt.%; and *downward-pointing triangles*, 1.0 wt.%. At the lower concentrations, $\tan\delta > 1$ and the material is predominantly viscous on the bulk scale, while at higher c, $\tan\delta < 1$ and it is elastic

addition, the moduli of the slow environment are one to two orders of magnitude larger than for the fast environment at the same concentration.

We also measured the bulk rheological behaviour of the Carbopol dispersions. As discussed above, we performed small-amplitude oscillatory shear measurements to determine the bulk viscous and elastic moduli $G_b''(\omega)$ and $G_b'(\omega)$ of the samples used in the particle-tracking measurements. Figure 7 shows the ratio $\tan\delta = G_b''/G_b'$ as a function of ω for Carbopol concentrations between 0.04 and 1.0 wt.%. All of these concentrations are above the threshold at which elastic effects are detectable in the particle tracking data discussed above. For $c < 0.05$ wt.%, $\tan\delta > 1$, meaning that the bulk material is predominantly viscous, while for $c \geq 0.1$ wt.%, $\tan\delta < 1$ and the dispersions are primarily elastic. For $c = 0.08$ wt.%, $\tan\delta \sim 1$ and is essentially independent of ω over the range of frequencies covered. This indicates a transition in the bulk material's state close to $c = 0.08$ wt.%. Both moduli show roughly a power-law dependence on frequency at concentrations around this value, and the frequency independence of the ratio $\tan\delta$ indicates that both have the same power-law exponent at the crossover. This behaviour is characteristic of a bulk-scale jamming transition in our dispersion near $c = 0.08$ wt.% (Prasad et al. 2003; Lally et al. 2007).

We compare the viscoelastic properties measured on the bulk and micron scales at a frequency of $\omega = 1$ rad/s in Fig. 8. The bulk elastic modulus G_b' is plotted along with G_m' for both the fast and slow populations in Fig. 8a. At the lowest concentrations, G_m' is too small to measure with our technique. In the vicinity of the bulk jamming transition, G_b' increases by two orders

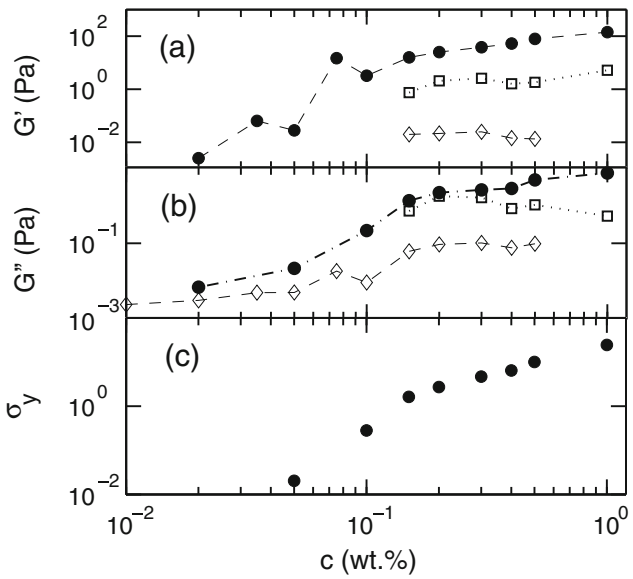

Fig. 8 Comparison of the bulk and microscopic viscoelastic properties. *a* $G'(\omega = 1$ rad/s) for the fast (*diamonds*) and slow (*squares*) populations and for the bulk (*solid circles*). The *lines* are for clarity. *b* The corresponding values of $G''(\omega = 1$ rad/s). *c* The yield stress σ_y determined from the bulk rheological measurements

of magnitude for only a factor of two increase in concentration. For $c > 0.15$ wt.%, it increases much more slowly. On the other hand, in the range of concentration over which they can be measured, the micron-scale elastic moduli of both the fast and slow environments appear to be constant within the experimental scatter. Both are significantly smaller than the bulk elastic modulus, which is an order of magnitude higher than the microscopic elastic modulus for the slow population, and about three orders of magnitude higher than the corresponding value for the fast population.

The bulk and microscopic viscous moduli are shown in Fig. 8b. At the lowest concentrations, the values of G'' measured on the two scales are similar, and appear to be approaching each other as the concentration decreases. Along with the fact that all of the tracer particles have $\alpha \approx 1$ at low concentrations, this suggests that the material is homogeneous at the lowest concentrations, as expected. Both the bulk and the microscopic viscous moduli increase with c, but with G''_b increasing more rapidly than G''_m. In the range of c in which two distinct populations are observed, the micron-scale viscous moduli for both populations are again constant within the scatter, while the bulk viscous modulus continues to increase slowly. In this range, G''_m for the slow population is comparable with the bulk value G''_b, while the viscous modulus for the fast population is significantly lower. The bulk and microscopic moduli measured at higher concentrations are clearly different. This, together with the bimodal distribution of α values discussed above, is a clear indication of heterogeneity of the material on the scale probed by the tracers for $c \gtrsim 0.15$ wt.%.

We also measured the flow curves, i.e. shear stress σ as a function of strain rate $\dot{\gamma}$, for our Carbopol dispersions. The data for each concentration were fit to the Herschel–Bulkley model, $\sigma = \sigma_y + k\dot{\gamma}^n$, to determine the bulk yield stress σ_y. Here, k, n, and σ_y are treated as material-dependent fitting parameters. σ_y is shown as a function of c in Fig. 8c. We find a measurable yield stress for $c \geq 0.05$ wt.%, approximately the same concentration at which a measurable elasticity appears in the particle tracking data and the concentration at which the data for G'_b and G''_b indicate a jamming transition.

Discussion

Our analysis of the viscosity of very low-concentration neutralized Carbopol dispersions suggests that the microgel particles expand by a factor of order 10 in diameter (10^3 in volume) on neutralization. This large swelling factor, which is consistent with the light scattering results of Lee et al. (2011), is no doubt a reason for the effectiveness of Carbopol as a rheology-modifying additive in consumer products. The Carbopol particles would be physically incapable of expanding to this extent if all of their polymer chains were heavily crosslinked, so a single expanded particle must mostly consist of almost-free, largely uncrosslinked polymer chains. We therefore interpret this result to indicate that at pH 6, the Carbopol particles have a strongly inhomogeneous structure, consisting of small, highly crosslinked regions (corresponding to the pH-independent half-micron length scale seen in the light scattering measurements) which do not swell significantly, surrounded by a network of much less-crosslinked polymer which does. We note that this structure is somewhat different from that of some other microgels that have been studied, which tend to be more uniformly crosslinked (Saunders and Vincent 1999; Pelton 2000; Cloitre et al. 2003a, b; Lyon et al. 2004; Das et al. 2006), as well as from previously published conceptualizations of the microstructure of Carbopol (Roberts and Barnes 2001; Piau 2007). Our tracer particles are much smaller than the size of the expanded network, but slightly larger than the highly crosslinked regions.

The inferred size of the microgel particles suggests that the volume fraction they occupy becomes of order 1 for a concentration on the order of a few times 10^{-2} wt.%. This is consistent with the concentration of 0.035 wt.% at which the diffusive exponent α starts to deviate from one, as seen in Fig. 1a, and also with the concentration of about 0.05 wt.% at which the bulk material becomes elastic and a measurable bulk yield stress appears. These two phenomena—the appearance of subdiffusive behaviour on the microscopic scale and the roughly simultaneous appearance of a yield stress on the macroscopic scale—indicate a jamming transition (Prasad et al. 2003) at which the Carbopol particles become kinetically trapped by contact or other interactions with their neighbours.

Based on our results, we can develop a picture of the microstructure of the Carbopol dispersion (Roberts and Barnes 2001; Cloitre et al. 2003a, b; Piau 2007) and relate it to the changes in bulk properties that accompany the jamming transition. At extremely low concentrations, the Carbopol is a homogeneous viscous fluid with similar properties on the bulk and micron scales. In this regime, the dispersion of swollen microgel particles appears as sketched schematically in Fig. 9a. It behaves essentially as a dilute suspension of hard spheres (Cloitre et al. 2003a, b), and the tracer particles move diffusively through it. At $c \approx 0.05$ wt.%

the motion of the tracer particles becomes slightly subdiffusive, while on the bulk scale the elastic modulus becomes larger than the viscous modulus and the material develops a yield stress. These phenomena all signal the jamming transition, at which point the Carbopol particles become kinetically arrested and unable to move through the dispersion. Since the individual Carbopol particles are extremely swollen, they consist essentially of water within an expanded network of polymer chains. The jamming that we observe is presumably due to a combination of steric interactions, entanglements, and possibly associative bonding involving these networks. This state is illustrated schematically in Fig. 9b.

The inhomogeneous structure of the individual microgel particles leads to heterogeneous dynamics of the suspended tracer particles within this jammed material.

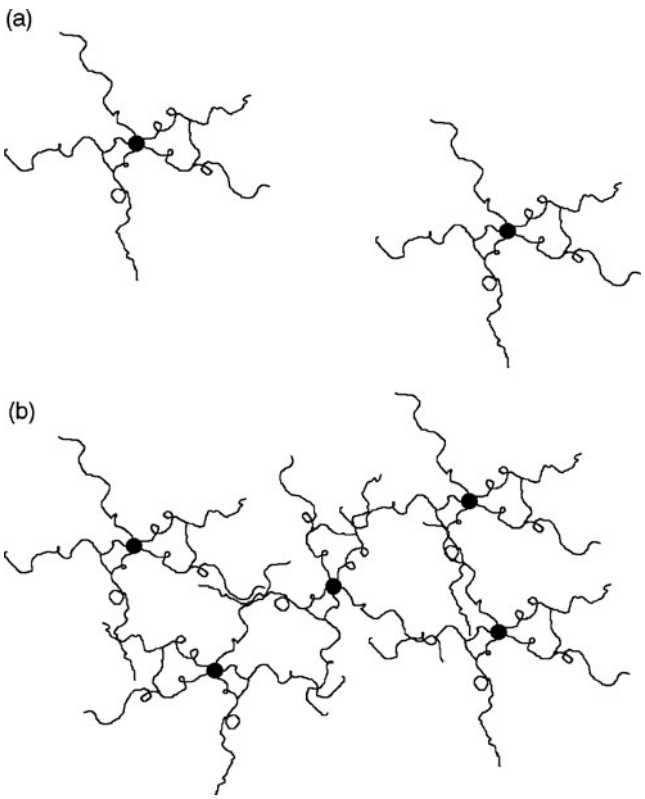

Fig. 9 A highly schematic illustration of the microstructure of Carbopol, as inferred from our measurements. At a pH of 6, the Carbopol particles are appear to consist of half-micron-sized regions of heavily crosslinked polymer—represented here by the *black dots*—surrounded by a highly expanded network of polymer chains. At low concentrations, illustrated in (**a**), the expanded Carbopol particles interact very weakly, if at all, and the dispersion is primarily viscous. **b** At higher concentrations, polymer chains from neighbouring Carbopol particles overlap, leading to a jamming of the Carbopol particles and resulting in a rheologically inhomogeneous microstructure

The tracer particles can undergo restricted diffusion in the solvent between the chains, even though the microgel particles themselves are jammed. As the concentration increases, the individual microgel particles are confined to a smaller volume and so are more compressed than at lower concentrations. This compression is manifested on the bulk scale by increases in the yield stress and the bulk elastic and viscous moduli. On the microscopic scale, it has been observed that compressed microgel particles develop a faceted shape (Cloitre et al. 2003a, b). Our particle tracking results indicate the appearance of a strongly viscoelastic rheological microenvironment as the concentration increases. We interpret this to indicate that some of the tracer particles—those in regions of the sample in which contacts or entanglements between Carbopol particles are more extensive, or where the microgel particles are more strongly compressed—experience significant elastic forces due to interactions with the polymer network. These particles form the slow population we observe. The fast population, on the other hand, consists of tracer particles moving through regions of the sample in which the polymer chains are less compressed or entangled. In these regions, the elastic effects of the polymer network are weaker and the tracer particles diffuse more freely. The decrease in slope at larger τ of the mean squared displacements of the individual particles shown in Fig. 2 indicates, however, that the size of these predominantly viscous regions is limited, and even the fast particles eventually become somewhat confined by the material (Oppong and de Bruyn 2007). In Fig. 9b, the "slow", more elastic regions are represented by the areas where chains are shown as overlapping, while the "fast", more viscous regions are those where no chains are shown. Figure 9 is of course highly schematic and should not be taken too literally. The structure and configuration of the microgel particles and the polymer chains in both regions is no doubt far less simple than drawn, but this basic structure is qualitatively consistent with the behaviour shown by our tracer particles.

The compression of the microgel particles as the Carbopol concentration is increased leads to an increase in the volume occupied by the elastic regions and a corresponding decrease in the volume of the less-entangled viscous regions. As a result, the number of slow tracers increases while the fast population declines, as observed. We also observe that the viscoelastic properties of the two environments do not depend significantly on concentration over the range that they coexist. This suggests that only the relative sizes of the viscous and elastic regions, and not their nature, change with c.

At $c \approx 1.0$ wt.% the elastic environment occupies essentially all of the sample. The abrupt change in

properties observed at this concentration may correspond to a bulk glass transition, although further work is needed to characterize this state. Nonetheless, our particle-tracking data suggest that at $c \approx 1.0$ wt.%, the Carbopol particles are more-or-less closely packed and compressed to the extent that the tracer particles are completely trapped within the polymer network. At this concentration (and presumably at higher c), the material is once again homogeneous on the micron length scale. The primarily viscous (fast) regions have been compressed out of existence, and the tracers are unable to diffuse at all. As c is increased further, the yield stress and bulk elastic modulus will continue to increase (Piau 2007), but any further changes to the microstructure would take place on length scales smaller than the size of our tracer particles and so would not be detectable in our particle-tracking measurements.

The combination of microrheological and bulk shear rheological measurements employed in this work has allowed us to make strong connections between the observed microscopic and macroscopic phenomena. These connections help to clarify our picture of the microstructure of Carbopol, and of how it changes as the Carbopol concentration is increased. While an understanding of microstructure and its relationship to bulk behaviour is arguably the goal of any fundamental study of soft materials, it is often difficult to achieve. We believe that the work presented in this paper provides an illustration of how microrheology can help us achieve this goal.

Conclusions

We have studied the micron-scale structure and rheology of suspensions of microgel particles as a function of concentration. We observe that the material undergoes a jamming transition at a particular microgel concentration. We have shown that two distinct micron-scale rheological environments coexist over a range of concentrations, and have related this result and the bulk rheological behaviour of the material to the structure of and interactions among the microgel particles in the vicinity of the jamming transition.

Acknowledgements We thank S. Sims for the use of his microscope and acknowledge useful discussions with P. Coussot and B. Frisken. This research was supported by NSERC of Canada.

References

Borrega R, Cloitre M, Betremieux I, Ernst B, Leibler L (1999) Concentration dependence of the low-shear viscosity of polyelectrolyte micro-networks: from hard spheres to soft microgels. Europhys Lett 47:729–735

Caggioni M, Spicer PT, Blair DL, Lindberg SE, Weitz DA (2007) Rheology and microrheology of a microstructured fluid: the gellan gum case. J Rheol 51:851–865

Cloitre M, Borrega R, Monti F, Leibler L (2003a) Glassy dynamics and flow properties of soft colloidal pastes. Phys Rev Lett 90:068303-1-4

Cloitre M, Borrega R, Monti F, Leibler L (2003b) Structure and flow behavior of polyelectrolyte microgels: from suspensions to glasses. C R Physique 4:221–230

Crassous JJ, Siebenbürger M, Ballauff M, Drechsler M, Henrich O, Fuchs M (2006) Thermosensitive core-shell particles as model systems for studying the flow behavior of concentrated colloidal dispersions. J Chem Phys 125:204906-1-11

Crocker JC, Grier DG (1996) Methods of digital video microscopy for colloidal studies. J Colloid Interface Sci 179: 298–310

Crocker J, Weeks E (2008) Particle tracking using IDL. Available at: http://www.physics.emory.edu/weeks/idl/index.html. Accessed 15 April 2010

Das M, Zhang H, Kumacheva E (2006) Microgels: old materials with new applications. Annu Rev Mater Res 36:117–142

de Bruyn JR, Oppong FK (2010) Rheological and microrheological measurements of soft condensed matter. In: Olafsen J (ed) Experimental and computational techniques in soft condensed matter physics. Cambridge University Press, Cambridge

Denton AR (2003) Counterion penetration and effective electrostatic interactions in solutions of polyelectrolyte stars and microgels. Phys Rev E 67:011804-1-10

Einstein A (1906) A new determination of molecular dimensions. Ann Physik 19:289–306

Gao Y, Kilfoil ML (2007) Direct imaging of dynamical heterogeneities near the colloid-gel transition. Phys Rev Lett 99:078301-1-4

Gardel ML, Valentine MT, Weitz DA (2005) Microrheology. In: Breuer K (ed) Microscale diagnostic techniques. Springer, New York

Gottwald D, Likos CN, Kahl G, Löwen H (2004) Phase behavior of ionic microgels. Phys Rev Lett 92:068301-1-4

Gottwald D, Likos CN, Kahl G, Löwen H (2005) Ionic microgels as model systems for colloids with an ultrasoft electrosteric repulsion: structure and thermodynamics. J Chem Phys 122:074903-1-11

Houghton HA, Hasnain IA, Donald AM (2008) Particle tracking to reveal gelation of hectorite dispersions. Eur Phys J E 25:119–127

Lally S, Mackenzie P, LeMaitre CL, Freemont TJ, Saunders BR (2007) Microgel particles containing methacrylic acid: pH-triggered swelling behaviour and potential for biomaterial application. J Colloid Interface Sci 316:367–375

Lee D, Gutowski IA, Bailey AE, Rubatat L, de Bruyn JR, Frisken BJ (2011) Investigating the microstructure of a yield-stress fluid by light scattering. Phys Rev E (to be published)

Levin Y, Diehl A, Fernández-Nieves A, Fernández-Barbero A (2002) Thermodynamics of ionic microgels. Phys Rev E 65:036143-1-6

Liu J, Gardel ML, Kroy K, Frey E, Hoffman BD, Crocker JC, Bausch AR, Weitz DA (2006) Microrheology probes length scale dependent rheology. Phys Rev Lett 96:118104-1-4

Lyon LA, Debord JD, Debord SB, Jones CD, McGrath JG, Serpe MJ (2004) Microgel colloidal crystals. J Phys Chem B 108:19099-19108

Mason TG, Weitz DA (1995) Optical measurements of frequency-dependent linear viscoelastic moduli of complex fluids. Phys Rev Lett 74:1250–1253

Mason TG (2000) Estimating the viscoelastic moduli of complex fluids using the generalized Stokes–Einstein equation. Rheol Acta 39:371–378

Noveon Technical Data Sheet 216 (2002) Available at: http://www.lubrizol.com/WorkArea//DownloadAsset.aspx?id=31922. Accessed 15 April 2010

Oppong FK, Rubatat L, Frisken BJ, Bailey AE, de Bruyn JR (2006) Microrheology and structure of a yield-stress polymer gel. Phys Rev E 73:041405-1-9

Oppong FK, de Bruyn JR (2007) Diffusion of microscopic tracer particles in a yield-stress fluid. J Non-Newton Fluid Mech 142:104–111

Oppong FK, Coussot P, de Bruyn JR (2008) Gelation on the microscopic scale. Phys Rev E 78:021405-1-10

Pelton R (2000) Temperature-sensitive aqueous microgels. Adv Colloid Interface Sci 85:1–33

Piau JM (2007) Carbopol gels: elastoviscoplastic and slippery glasses made of individual swollen sponges Meso- and macroscopic properties, constitutive equations and scaling laws. J Non-Newton Fluid Mech 144:1–29

Prasad V, Trappe V, Dinsmore AD, Segre PN, Cipelletti L, Weitz DA (2003) Universal features of the fluid to solid transition for attractive colloidal particles. Faraday Discuss 123:1–12

Roberts G, Barnes HA (2001) New measurements of the flow-curves for Carbopol dispersions without slip artefacts. Rheol Acta 40:499–503

Saunders BR, Vincent B (1999) Microgel particles as model colloids: theory, properties and applications. Adv Colloid Interface Sci 80:1–25

Senff H, Richtering W (1999a) Rheology of a temperature sensitive core-shell latex. Langmuir 15:102-106

Senff H, Richtering W (1999b) Temperature sensitive microgel suspensions: colloidal phase behavior and rheology of soft spheres. J Chem Phys 111:1705–1711

Tabuteau H, Coussot P, de Bruyn JR (2007) Drag force on a sphere in steady motion through a yield stress fluid. J Rheol 51:125–137

Valentine MT, Kaplan PD, Thota D, Crocker JC, Gisler T, Prud'homme RK, Beck M, Weitz DA (2001) Investigating the microenvironments of inhomogeneous soft materials with multiple particle tracking. Phys Rev E 64:061506-1-9

Wong IY, Gardel ML, Reichman DR, Weeks ER, Valentine MT, Bausch AR, Weitz DA (2004) Anomalous diffusion probes microstructure dynamics of entangled F-actin networks. Phys Rev Lett 92:178101-1-4

Waigh TA (2005) Microrheology of complex fluids. Rep Prog Phys 68:685–742

Wu J, Zhou B, Hu Z (2003) Phase behavior of thermally responsive microgel colloids. Phys Rev Lett 90:048304-1-4

Yu Q, Kaloni PN (1988) A note on the suspension viscosity of porous spherical particles. ZAMP 39:937–941